

Research Article

Xinyu Hu, Rui Pan, Mingyong Cai, Weijian Liu, Xiao Luo, Changhao Chen, Guochen Jiang and Minlin Zhong*

Ultrafast laser micro-nano structured superhydrophobic teflon surfaces for enhanced SERS detection via evaporation concentration

<https://doi.org/10.1515/aot-2019-0072>

Received December 25, 2019; accepted March 4, 2020; previously published online April 28, 2020

Abstract: Evaporation concentration of target analytes dissolved in a water droplet based on superhydrophobic surfaces could be able to break the limits for sensitive trace substance detection techniques (e.g. SERS) and it is promising in the fields such as food safety, eco-pollution, and bioscience. In the present study, polytetrafluoroethylene (PTFE) surfaces were processed by femtosecond laser and the corresponding processing parameter combinations were optimised to obtain surfaces with excellent superhydrophobicity. The optimal parameter combination is: laser power: 6.4 W; scanning spacing: 40 μm ; scanning number: 1; and scanning path: 90 degree. For trapping and localising droplets, a tiny square area in the middle of the surface remained unprocessed for each sample. The evaporation and concentration processes of droplets on the optimised surfaces were performed and analyzed, respectively. It is shown that the droplets with targeted solute can successfully collect all solute into the designed trapping areas during evaporation process on our laser fabricated superhydrophobic surface, resulting in detection domains with high solute concentration for SERS characterisation. It is shown that the detected peak intensity of rhodamine 6G with a concentration of 10^{-6} M in SERS characterisation can be obviously enhanced by one or two orders of magnitude

on the laser fabricated surfaces compared with that of the unprocessed blank samples.

Keywords: concentration; evaporation behaviour; femtosecond laser; PTFE; superhydrophobicity.

OCIS Codes: 140.7090; 160.5470; 240.6695

1 Introduction

Inspired by nature, superhydrophobic surfaces like lotus-leaves (which are generally with contact angle (CA) larger than 150° and sliding angle (SA) smaller than 10°) have attracted extensive attention and exhibit great potential applications in the fields like self-cleaning [1], drag reduction, [2] and water collection [3]. To quantify a surface's superhydrophobicity, two indexes, CA and SA, are proposed and normally used. Generally, a great superhydrophobicity is characterised by a high CA and a low SA. The droplets on such a superhydrophobic surface is very mobile and can roll off the surface very easily [4]. Droplets on a surface can exhibit high CAs with two main possible wetting states, the Cassie-Baxter state and the Wenzel state. In Cassie-Baxter state, air pockets are trapped as cushions within the surface micro-nano structures between the solid and the water droplet. Thus, the real contact area between the solid and the liquid is actually less than the apparent area. In contrast, in Wenzel state, the droplet pins to the rough surface and wets the solid surface completely. However, A Cassie-Baxter state always shows much lower SAs than a Wenzel state, because of its smaller solid-liquid contact area and contact angle hysteresis [5].

Although the wetting state of a droplet placed on a superhydrophobic surface is mainly determined by the surface's topography and chemistry, the transition from Cassie-Baxter state to Wenzel state can also be triggered

*Corresponding author: Minlin Zhong, Laser Material Processing Research Center, School of Materials Science and Engineering, Tsinghua University, Beijing 100084, China, e-mail: zhml@tsinghua.edu.cn

Xinyu Hu, Rui Pan, Mingyong Cai, Weijian Liu, Xiao Luo, Changhao Chen and Guochen Jiang: Laser Material Processing Research Center, School of Materials Science and Engineering, Tsinghua University, Beijing 100084, China. <https://orcid.org/0000-0001-7477-5093> (R. Pan)

www.degruyter.com/aot

© 2020 THOSS Media and De Gruyter

under certain circumstances, e.g. vibrations, squeezing, impact and evaporation [5, 6], resulting in a surface with a high adhesion (to water) and losing its superhydrophobicity. Hence, a good Cassie-Baxter state stability is very important for a superhydrophobic surface in practice. Droplet evaporation experiment is one of the most common methods to evaluate superhydrophobic surfaces' Cassie-Baxter state stability. During evaporation, the volume of the droplet decreases based on either a constant contact radius (CCR) evaporation mode or a constant contact angle (CCA) evaporation mode or a mixed mode [7, 8]. The Laplace pressure generated on the surface of the droplet increases gradually with the decrease in droplet radius. When the volume of the droplet reduces to a certain degree, the increasing Laplace pressure exceeds the critical Laplace pressure that the surface could sustain, triggering the transition from Cassie-Baxter state to Wenzel state. Due to the transition, the liquid intrudes into the surface asperities and the resultant solid-liquid contact area increases greatly, which significantly enhances the adhesion between the surface and the droplet. The three-phase contact line (TPCL) is then pinned into the surface asperities and the droplet evaporation conforms to the CCR mode or a mixed model until the droplet completely evaporates [5–14].

The evaporation of a droplet on a superhydrophobic surface with great Cassie-Baxter state stability results in a small final solid-liquid contact area when the transition from Cassie-Baxter to Wenzel state happens. Such a phenomenon inspires a novel way to concentrate solute in a solution droplet. A droplet on a superhydrophobic surface will shrink and collect all solute into a diminutive zone with a much higher concentration after the evaporation process. Smaller ultimate solid-liquid contact areas imply more efficient and higher concentration of the solute. The concentration based on superhydrophobic surfaces has been combined with various kinds of detection methods, e.g. surface-enhanced Raman spectroscopy (SERS) and surface-enhanced photoluminescence (SEPL), to detect the existence of trace substances [15–28]. Due to the advantages of low cost, high efficiency and mild operating condition, these combined techniques have been attracting extensive attention of researchers and are promising in food safety, environment monitoring, [15] and biomedicine [17]. McHale et al. have studied the evaporation behaviour of droplets on patterned polymer surfaces and found the contact line's stepwise jumping receding and the abrupt collapse of the droplet during evaporation [9]. Zhang et al. electrodeposited flower-like 3D Ag nanostructures on indium tin oxide glasses and then gained flower-like 3D Ag-Au hetero-nanostructures by galvanic

replacement reaction, which played an important role in enhancing SERS characterisation [18]. Shi et al. deposited gold nanoislands on the dragonfly wings via a DC magnetron sputtering system as an enhancing SERS substrate and a 10^{-7} M Rhodamine 6 G (R6G) was detected [20]. De Angelis et al. obtained various superhydrophobic SERS and SEPL substrates of Si wafers and the prepared substrates could be able to detect a single DNA molecule [26]. Zhizhchenko et al. successfully detected the existence of 10^{-10} M R6G by concentrating droplets on a polytetrafluoroethylene (PTFE) substrate with a hierarchical structure prepared by femtosecond laser assisted with electron-beam processing [29].

As stated above, several methods with diverse materials have been attempted to fabricate substrates to realise high-degree concentration and enhancement for trace substance detection. However, all these methods have their intrinsic constraints, such as complex procedures, expensive facilities, involving dangerous chemicals, and dependence on material types. Alternatively, ultrafast laser is a powerful tool for surface processing of almost every solid material. Rare work about PTFE as a concentration substrate simply fabricated by an ultrafast laser direct-writing process has been done. In this study, a facial and simple method is proposed to fabricate PTFE blocks by femtosecond laser to obtain superhydrophobic surfaces with great Cassie-Baxter state stability. A tiny hydrophobic zone was remained unprocessed in the middle of the surface to localise solution droplet placed on it during evaporation. The wettability, evaporation behaviour, and concentration results of different PTFE surfaces are systematically studied and optimised in the present study. It is shown that our prepared surface could be able to realise efficient concentration and distinct characteristic peaks can be detected for 10^{-6} M R6G by SERS. The peak intensity that our prepared surface could be able to detect is one to two orders of magnitude stronger than that of the blank sample.

2 Materials and methods

2.1 Fabrication of superhydrophobic surfaces

The commercially available PTFE samples (with a size of $30 \times 30 \times 3$ mm³) employed in this study were first polished with 600 and 1500 mesh sandpapers, respectively. Then they were ultrasonically washed with ethanol solution for 5 minutes at room temperature and dried by a compressed Nitrogen flow. Next, the surface structure was fabricated by a Trumpf TruMicro 5000 laser system with 800 fs pulses and 1030 nm central wavelength. To focus and

scan the laser beam in the x-y direction, a two-mirror galvanometric scanner with an F-Theta objective lens of 100 mm focus length was used. The focused diameter of the Gaussian-profile laser beam at $1/e^2$ of its maximum intensity was 30–35 μm . During the laser direct writing process, scanning speed and repetition frequency were fixed at 100 mm/s and 200 kHz, respectively. The adjusted parameters and their varying ranges were laser power (1.6–9.6 W), scanning interval (40–50 μm), scanning number (1–3 times) and scanning path (named as 90° and 60°, as shown in Figure 1A). The entire surface of each sample was ablated by the laser to become superhydrophobic except for a tiny square domain in the middle of each sample (as shown in Figure 1C). The tiny domain remained unprocessed as a hydrophobic surface to trap and fix the droplet in that area during evaporation and concentration. The side length of the square unprocessed area is designed to be 235 μm . In SERS experiments, a 5 μl mixed solution comprised of Au sol and R6G solution of various concentrations was positioned and trapped above the unprocessed domain (as shown in Figure 1C), where the laser illuminates during SERS experiments after the evaporation.

2.2 Reagent preparation

Au sol solution with original concentration of 0.05 mg/ml (commercially available from Shanghai So-Fe Biomedical Co., Ltd.) was used as received. The gold nanoparticles in the Au sol solution are with an average diameter of about 10 nm. Then, such an original Au sol solution was diluted with deionised water to 10^{-6} mol/l. Then the diluted Au sol solution was stored at 4°C in vacuum.

R6G bought from Shanghai Macklin Biochemical Co., Ltd. were used as received, dissolved in deionised water to prepare R6G solution with various concentrations, including 10^{-6} mol/l, 10^{-8} mol/l, 10^{-8} mol/l and 10^{-10} mol/l.

2.3 Characterisation methods

The morphology of the prepared surface was characterised by Olympus LEXT OLS4100 laser scanning confocal microscopy (LSCM) and FEI Quanta 200FEG SEM. The superhydrophobicity of the prepared surface was characterised by CA and SA and measured by a Data-physics OCA 15 Plus video-based optical contact angle measuring device (OCA) with a tilted platform using a sessile drop method. A 5 μl of deionised water was used for CA and SA measurement. Samples with sufficiently good superhydrophobicity were chosen to perform the evaporation experiments. The evaporation experiments were performed at 25–30°C on the same OCA device with the CCD camera turned on to record the droplet profile during evaporation process of a 5 μl deionised water droplet on a prepared surface (shown as Figure 1B). Since efficient concentration suggests small final contact area, samples with small size of ultimate contact zones were remained for subsequent experiments. In the concentration experiments, a 5 μl droplet of 10^{-6} mol/l Au sol solution was positioned on a sample surface and evaporated naturally in air. After evaporation, the morphology of the concentration area on the sample was observed by LSCM to check and evaluate the quality of the concentration process. In the SERS experiments, 5 μl of a mixed solution, which was a R6G solution with a series of different concentrations mixed with a 10^{-6} M Au sol solution by a volume ratio of 5:1, was

positioned and evaporated on clean prepared sample surfaces. Then the samples were detected by a Horiba LabRAM HR Evolution Laser Raman spectrometer with a 633 nm laser source from 600 cm^{-1} to 1900 cm^{-1} . During each SERS measurement, laser scanning was done five times in total eight seconds. Droplets were all placed exactly on the unprocessed hydrophobic zone in the evaporation experiments, the concentration experiments and the SERS experiments.

3 Results and discussion

3.1 Morphology and superhydrophobicity of the prepared surfaces

As can be seen in Figure 2, hierarchical surface structures, which are composed of microcolumn arrays with unique nanostructures, are obtained on PTFE after laser ablation. The microcolumns are attached with various nanoparticles and the nanoparticle clusters form nanoholes, nanobulges, and nanogullies. Nanowires can also be observed between the nanoparticles when the laser power is smaller than 4.0 W and the scanning number is only 1, as shown in Figure 2E(i).

The morphology and distribution of the microcolumns fabricated with different laser process parameters are shown in Figure 2E. As can be seen, the morphology of the microcolumns changes apparently with the varied process parameters. The scanning path determines the distribution and shape of microcolumns and the scanning spacing influences the periodicity of the microcolumns, while the laser power and the scanning number mainly impacts the height and the shape of the microcolumns. As shown in Figures 2E and 3A, when the scanning interval is fixed at 50 μm and the scanning path is 90°, the height of the obtained microcolumns gets higher and the shape of them gets rounder and lankier as the laser power increases from 1.6 W to 9.6 W and the scanning number increases from 1 to 3 times. In most cases, the microcolumns are in regular shapes and distributed uniformly. However, when the scanning number is more than 2 and the scanning power is larger than 4.0 W for samples with 60° scanning path and 40 μm scanning period, the height of the obtained microcolumns unusually decreases with further increase in the scanning number and scanning power and the resultant surface microstructures become unshaped, disordered, and randomly distributed, as shown in Figure 2E(v). The decreasing height of the resultant microcolumns can be ascribed to the over-ablation and melting of the surface structure. This phenomenon is easier to occur when reducing the scanning interval or adding the scanning number at the same point. Samples

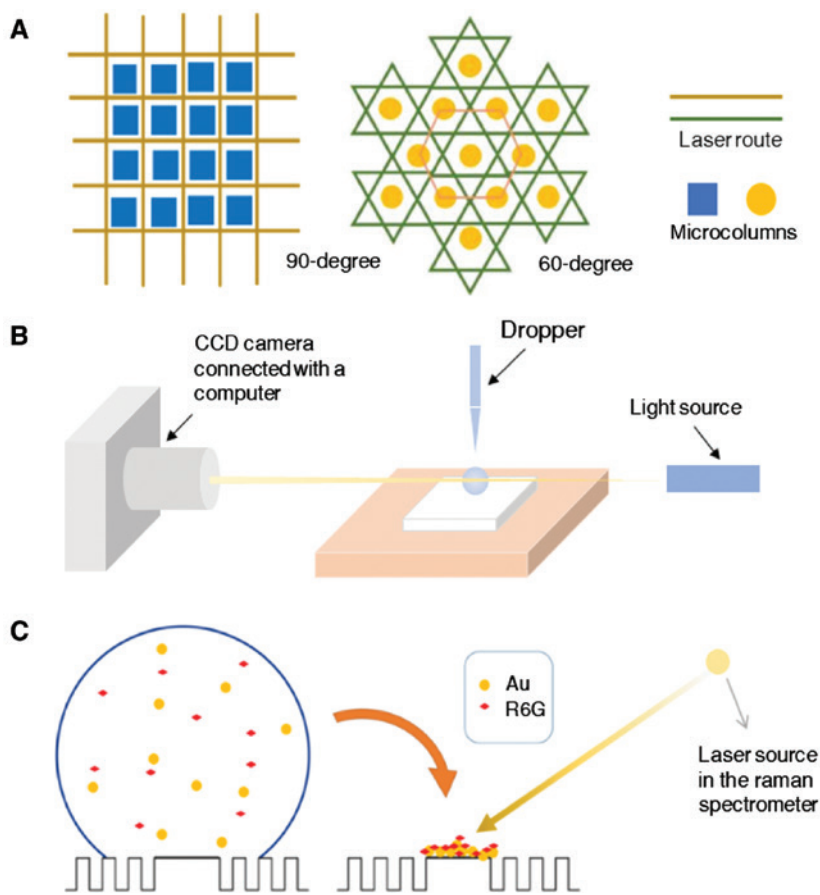


Figure 1: The diagrams of two laser scanning paths (A), schematic of evaporation experiments (B) and the preparation of SERS samples (C).

with extremely uneven surface microstructures, which are not able to measure the height of microcolumns, are not plotted in Figure 3A. The microcolumns with the scanning path of 60° are higher than those of 90° in the same condition, owing to one more scanning at the same position. The foregoing unprocessed hydrophobic zone is shown in Figure 2C, and its actual side length is approximately $235\ \mu\text{m}$ for all the samples.

The dependence of CAs and SAs of the processed surfaces on different laser processing parameters is shown in Figure 3B. Compared with the unprocessed PTFE sample (whose CA is about 110° and SA is above 180° , i.e. the droplet doesn't roll off the surface even when the surface is turned up-side-down), the laser processed PTFE samples have remarkable improvements in superhydrophobicity. Overall, it can be observed that the CAs of all the surfaces fabricated by different parameters are generally larger than 150° , while the SA varies between 2° and 40° in a wide range without a clear trend with the changes of different processing parameters. Specifically, the comprehensive superhydrophobicity improves a lot when the scanning interval changing

from $50\ \mu\text{m}$ to $40\ \mu\text{m}$, due to the decreased periodicity of the microcolumns and the resultant surface roughness. Since the limitation of our laser spot diameter is $30\ \mu\text{m}$, the surfaces ablated with smaller scanning interval are not prepared and discussed in this work. However, both CAs and SAs of the prepared surfaces don't change obviously with the scanning path changing from 90° to 60° and the scanning number ranging from 1 to 3 times. Most samples with hybrid surface structures of complete well-distributed microcolumns covered with nanoparticles have attained at least high CAs, while the over-ablated samples with seriously uneven surface structures have their CAs drop to about 142° , as shown in Figure 3B xi and xii.

The average values of the contact and sliding angles for each sample were determined by five measurements, at different randomly selected locations on each sample's surface. The standard deviation of the measured CAs is less than 3° for $\text{CA} \geq 150^\circ$.

Since a good concentration behaviour requires the surface to have a great Cassie-Baxter state stability, which implies excellent superhydrophobicity and extremely

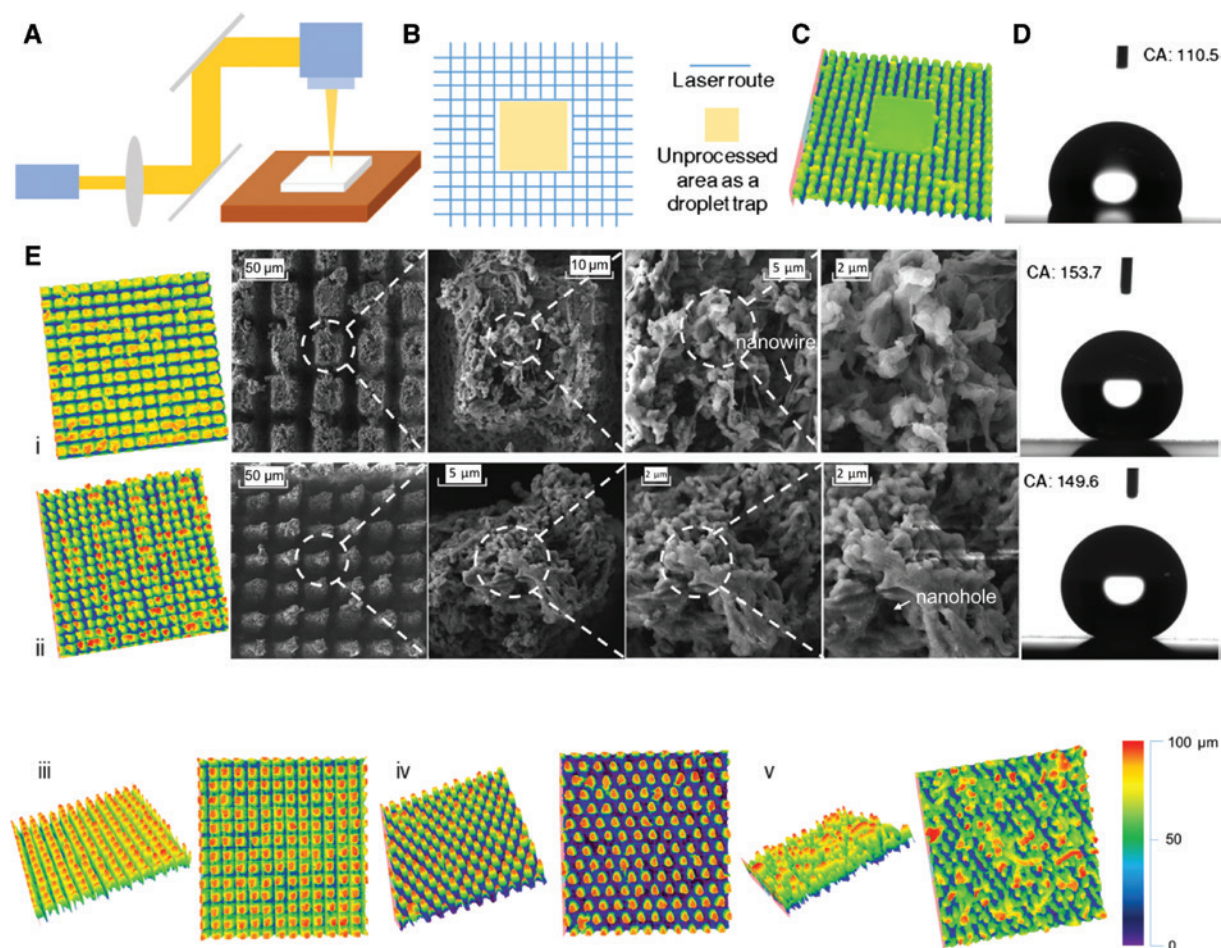


Figure 2: Schematic of laser processing (A), fabrication of droplet trapping zone (B) with its microscale morphology (C), CA of droplets on an unprocessed clean PTFE surface (D), surface LSCM topographies of samples and the corresponding color scale, with the SEM micrographs and the side-profile images of 5 µl droplets on surfaces for samples in i. and ii. (E) (i. 4.0 W, 50 µm, 90°, scanning once; ii. 5.6 W, 50 µm, 90°, scanning twice; iii. 7.2 W, 50 µm, 90°, scanning 3 times; iv. 5.6 W, 50 µm, 60°, scanning 3 times; v. 7.2 W, 40 µm, 60°, scanning once).

weak adhesion to droplets [10, 11], and high efficiency is preferred, the samples fabricated with the optimised processing parameter combinations ‘3.6–4.4 W, 50 µm, 90° 1’, ‘5.2–6.0 W, 50 µm, 90°’ and ‘3.6–6.8 W, 40 µm, 90°, 1’ were chosen for subsequent experiments. The detailed parameters of the chosen samples are listed in Table 1.

3.2 Evaporation behaviour

A 5 µl deionised water droplet was positioned on the tested sample surface and its evaporation process was recorded and analyzed. For comparison, the evaporation processes of droplets on the original sample and the laser-fabricated samples are recorded, respectively. The CAs, SAs, and the diameters of the ultimate contact area are measured, as shown in Table 1.

The volume of droplet is calculated based on the spherical cap approximation and the real-time side profile image taken from the videos recorded by the CCD camera [9, 12]. Detailed information for the droplets’ volume calculation and the diameter of the contact area measurement is shown in Supplementary Materials.

The evaporation behaviour of the droplet on an unprocessed hydrophobic PTFE sample is shown in Figure 4A (recorded as Movie S1, in the Supplementary Materials). As can be seen, the volume of the droplet decreases fast at first. Then it gradually slows down with the proceeding of evaporation process. This is because the reduction of the droplet volume results in the reduction of the vapor and liquid contact area, which limits the diffusion of the gasified liquid into ambient environment [10]. Based on Figure 4A(ii), the evaporation process on the unprocessed PTFE samples can be divided into three stages. The first stage is a CCR mode where the diameter of the contact

area stays basically unchanged and the CA constantly declines. Then the second stage is a quasi-CCA mode, i.e. the contact area shrinks apparently while the CA only changes little in this stage. The last stage is a mixed stage, where both the contact area and the CA change simultaneously, but the latter changes faster. During this stage, the droplet will finally pin to the surface. It is observed that the diameter of the solid-liquid contact area finally pinned to the surface is about $650\ \mu\text{m}$. Based on the evaporation models, an explanation of the evaporation behaviour is proposed as follows. The first stage occurs, because the pinning force of the droplet's TPCL derived from the adhesion of the surface is stronger than the initial depinning force derived from the unbalanced system's surface tension [5, 29]. The depinning force gets stronger as the CA decreases and gradually reaches to a critical value where the depinning force is comparable with the pinning force. Then the droplet's evaporation enters the second quasi-CCA stage, where the CA only needs to change a little, but the TPCL has to retreat a lot to keep the balance. Finally, with the proceeding of evaporation, the volume of the droplet becomes so small that the droplet volume changes

at a particular fast rate. As a result, the TPCL cannot shrink in time to remain the droplet as a segment and both the CA and TPCL decrease obviously at this stage.

The evaporation behaviour of the droplets on laser-processed superhydrophobic PTFE surfaces are shown in Figure 4B and C (recorded as Movie S2 and S3, respectively, in the Supplementary Materials). The evaporation curves in Figure 4B(i) and C(i) are similar to that in Figure 4A(i). However, due to the superhydrophobicity, the laser fabricated samples exhibit higher evaporation speed on account of their stronger ability to maintain the droplet in a sphere shape and with a larger vapor-liquid contact area. Such an evaporation process can be roughly divided into two stages. The first stage occupies most of the time and present a periodic jagged CA changing curve and a step-by-step diminishing TPCL diameter changing curve, as shown in Figure 4B(ii) and C(ii). The time at which the diameter changes is exactly the time when the CA changes from the local minima to the local maxima. Each time the more the diameter changes, the more the CA recovers. In this stage, with the decline of the droplet volume, the TPCL is pinned to the surface and the CA

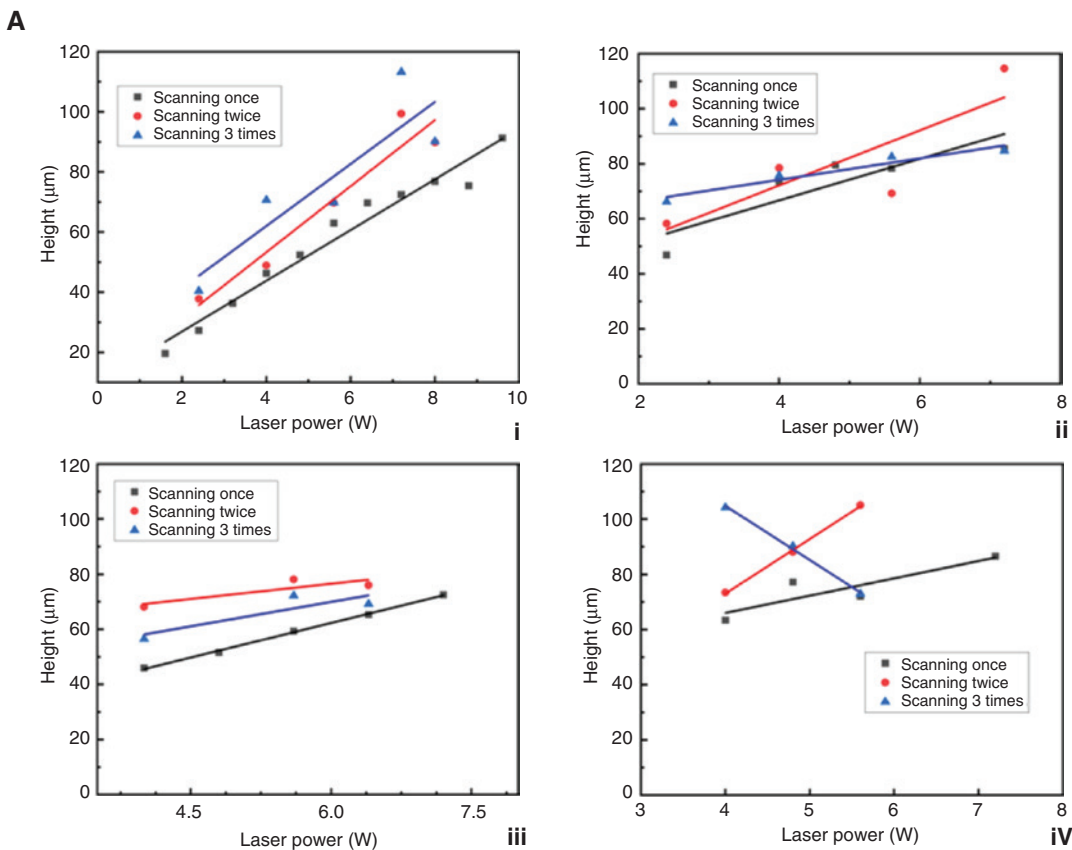


Figure 3: The variation of the microcolumns' height with processing parameters (A) (i. $50\ \mu\text{m}$, 90° ; ii. $40\ \mu\text{m}$, 90° ; iii. $50\ \mu\text{m}$, 60° ; iv. $40\ \mu\text{m}$, 60°) and the CAs and SAs of samples with different parameter combinations, the units of SA axes (the left ones) and CA axes (the right ones) are both degree (B).

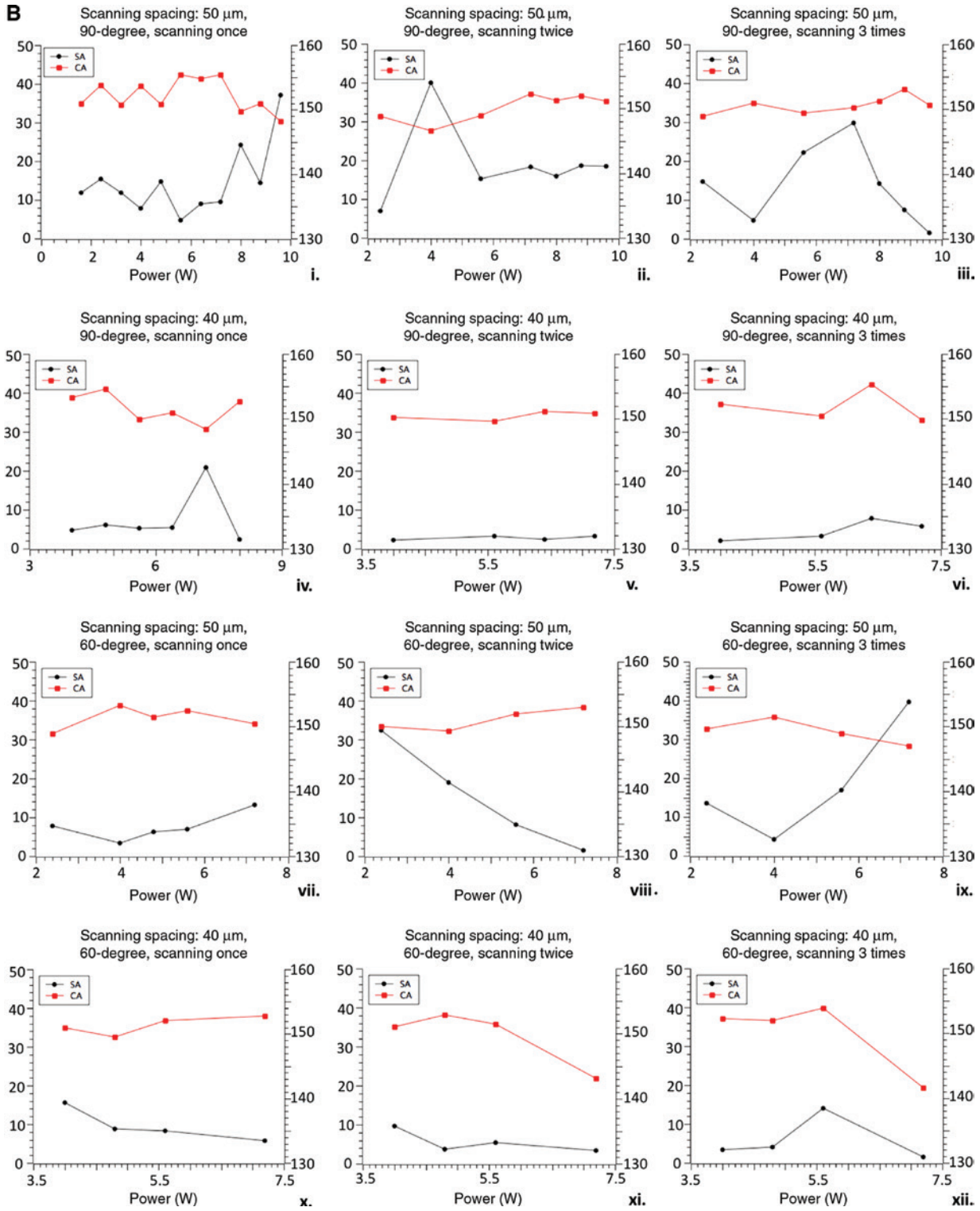


Figure 3 (continued)

decreases gradually at the beginning. According to the calculation model from De Angelis et al. [26], the adhesion pinning force F_p along one direction on a superhydrophobic surface can be calculated as follows:

$$F_p = 2r\gamma_{lv}(\cos\theta_r - \cos\theta_a)\varphi_s \quad (1)$$

where r is the radius of the TPCL, γ_{lv} is the surface tension between the liquid and the solid, φ_s is the fraction of solid

Table 1: The parameters and measured data for samples in evaporation experiments.

Sample	Laser power	Scanning number	Scanning path	Scanning interval	CA/degree	SA/degree	Ultimate diameter/ μm
Unprocessed PTFE	/	/	/	/	110	>180	650
1	3.6	1	90°	50 μm	/	/	389
2	4.0	1	90°	50 μm	153.7	7.8	371
3	4.4	1	90°	50 μm	/	/	253
4	5.2	1	90°	50 μm	/	/	302
5	5.6	1	90°	50 μm	155.4	4.7	234
6	6.0	1	90°	50 μm	/	/	284
7	3.6	1	90°	40 μm	/	/	350
8	4.0	1	90°	40 μm	153.3	4.8	282
9	4.4	1	90°	40 μm	/	/	348
10	4.8	1	90°	40 μm	154.6	6.1	240
11	5.2	1	90°	40 μm	/	/	300
12	5.6	1	90°	40 μm	149.9	5.3	249
13	6.0	1	90°	40 μm	/	/	258
14	6.4	1	90°	40 μm	150.9	5.5	216
15	6.8	1	90°	40 μm	/	/	324

in contact with liquid, θ_r and θ_a are the receding contact angle and the advancing contact angle, respectively, and $\cos \theta_r - \cos \theta_a$ is related to the SA of the surface. At the same time, the system deviates from the equilibrium state and forms an increasing inward depinning force. The depinning force F_d can be evaluated as the following equation [26]:

$$F_d = 2r\gamma_{lv}(\cos\theta - \cos\theta_e) \quad (2)$$

where θ is the real CA and θ_e is the equilibrium CA. When θ decreases to a certain extent, F_d increases and equals to F_p and the TPCL suddenly retreats one or more intervals of the microcolumns. As a result, the CA abruptly increases and the system recovers to a relatively equilibrium state, which is the start of another cycle [12, 13, 24, 26]. Such cycles are exactly the phenomenon presented on the tested superhydrophobic surface prepared in this present study during the droplet evaporation process. This stage can be regarded as a CCA mode [11, 29]. The second stage only lasts for a short period of time before the evaporation process ends. This stage shows a CCR mode where the TPCL is pinned and the CA declines quickly, indicating that the transition from Cassie-Baxter to Wenzel state is triggered by the increased Laplace pressure with the decreasing droplet radius during evaporation process. The demarcation point of the two stages is an evident salient point which indicates the transition [29]. Once the TPCL retreats to the unprocessed hydrophobic zone mentioned in Section 2.1, it gets pinned and stops moving.

Comparing Figure 4B and C, sample surfaces fabricated by different laser processing parameters exhibit little differences in their evaporation curves. The

evaporation curves with delayed Cassie-Baxter to Wenzel state transition points and more frequent leaps in the first stage indicate a better Cassie-Baxter state stability of the surfaces. Such a surface is more likely to obtain a smaller final contact area after the evaporation. The diameters of the contact areas at the transition points of the samples with greater Cassie-Baxter state stability (as the sample in Figure 4B) is close to the sizes of the designed trapping zones. This suggests that the droplets tend to collapse when their contact areas shrink to the designed domains.

Based on the theory of Kusumaatmaja et al. [6], the critical droplet radius of Cassie-Baxter to Wenzel state transition on sample surfaces with high enough microcolumns is decided by the spacing between the microcolumns d and the CA of the flat surface θ_f [6, 26]:

$$r_{cri} = d / \cos\theta_f \quad (3)$$

In the present study, θ_f is 110° as measured on the unprocessed PTFE surface, d is selected as 50 μm and 40 μm , respectively. According to (3), the corresponding r_{cri} is approximately 146 μm and 117 μm , respectively. However, the actual diameter of droplets when the transition happens is $316.5 \pm 59.2 \mu\text{m}$ and $287.4 \pm 48.3 \mu\text{m}$, respectively, which is larger than the calculated values. This might be due to the existence of the unprocessed trapping domain on the prepared surface, and/or the differences between the shapes of the fabricated microcolumns in the present study and the assumed posts in H. Kusumaatmaja's study.

The uncertainty in angle evaluation is smaller for high angles and larger for low angles. The standard deviation of the measured CAs is less than 3° for $\text{CA} \geq 150^\circ$ and

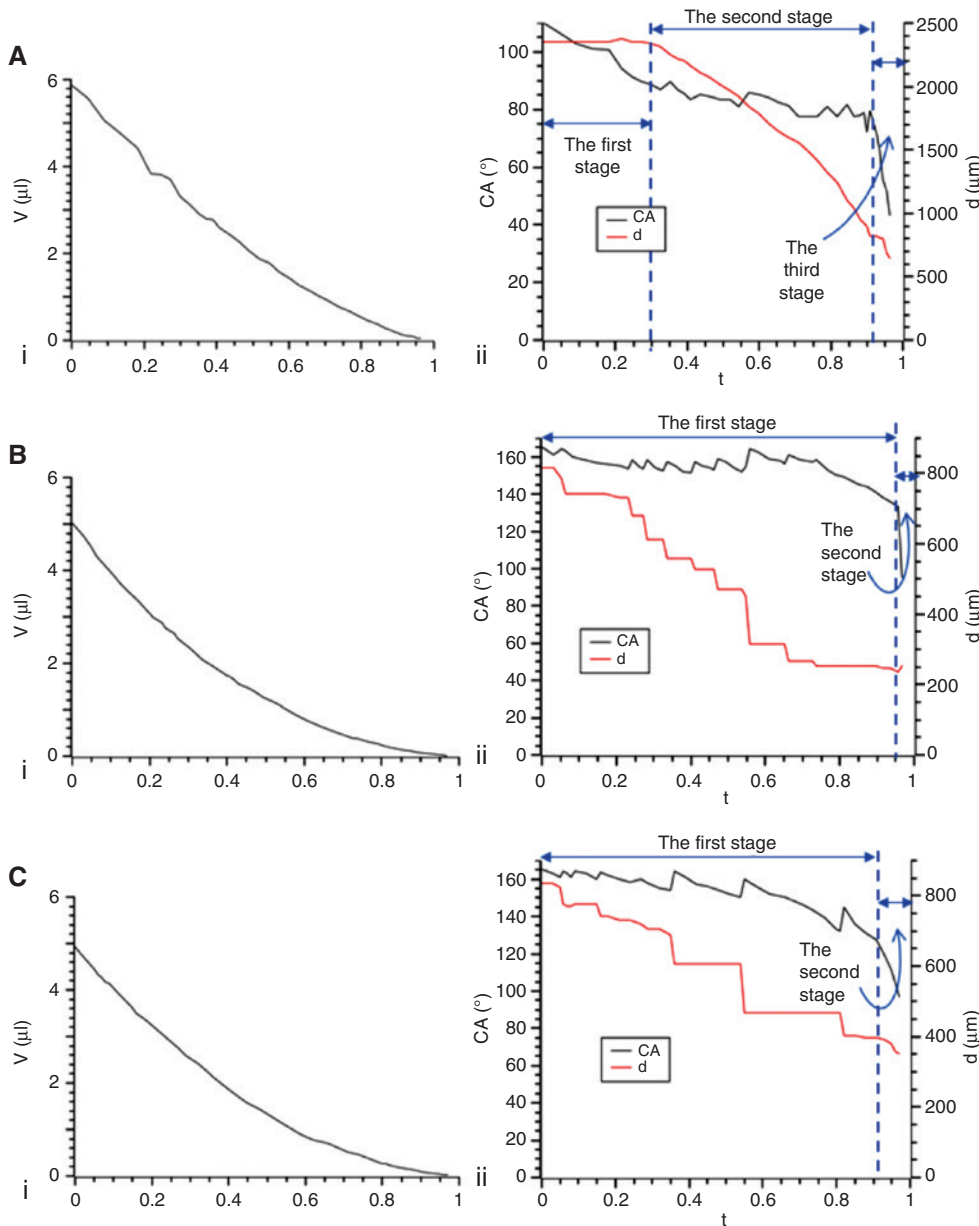


Figure 4: The evaporation behaviour of droplets on an original PTFE sample surface (A), and on laser-processed sample surfaces with processing parameter combinations ‘4.4 W, 50 μm , 90 $^\circ$, scanning once’ (B) and ‘3.6 W, 40 μm , 90 $^\circ$, scanning once’ (C), respectively.

around 5 $^\circ$ for $CA \leq 135^\circ$. The uncertainty in TPCL diameter evaluation is 0.002–0.03 mm (average standard deviation is 0.02 mm).

A small final size of the contact area is essential for efficient solute concentration. On account of this criterion, samples named 3, 4, 5, 6, 8, 9, 10, 11, 12, 13, 14 and 15 in Table 1 are selected to continue the concentration and SERS experiments. The optimal sample is number 14 with its parameter combination: laser power: 6.4 W; scanning spacing: 40 μm ; scanning number: 1; and scanning path: 90 $^\circ$.

3.3 Evaporation concentration experiments and SERS detection

Firstly, a 5 μl droplet of 10 $^{-6}$ mol/l Au sol solution was evaporated on different surfaces to inspect whether the processed surfaces can efficiently concentrate all solute of the droplet into the designed hydrophobic zone. The results are shown in Figure 5A, C and D.

As can be seen in Figure 5A, after the evaporation concentration process, a distinct coffee ring is left on the unprocessed sample surface. The formation of the coffee

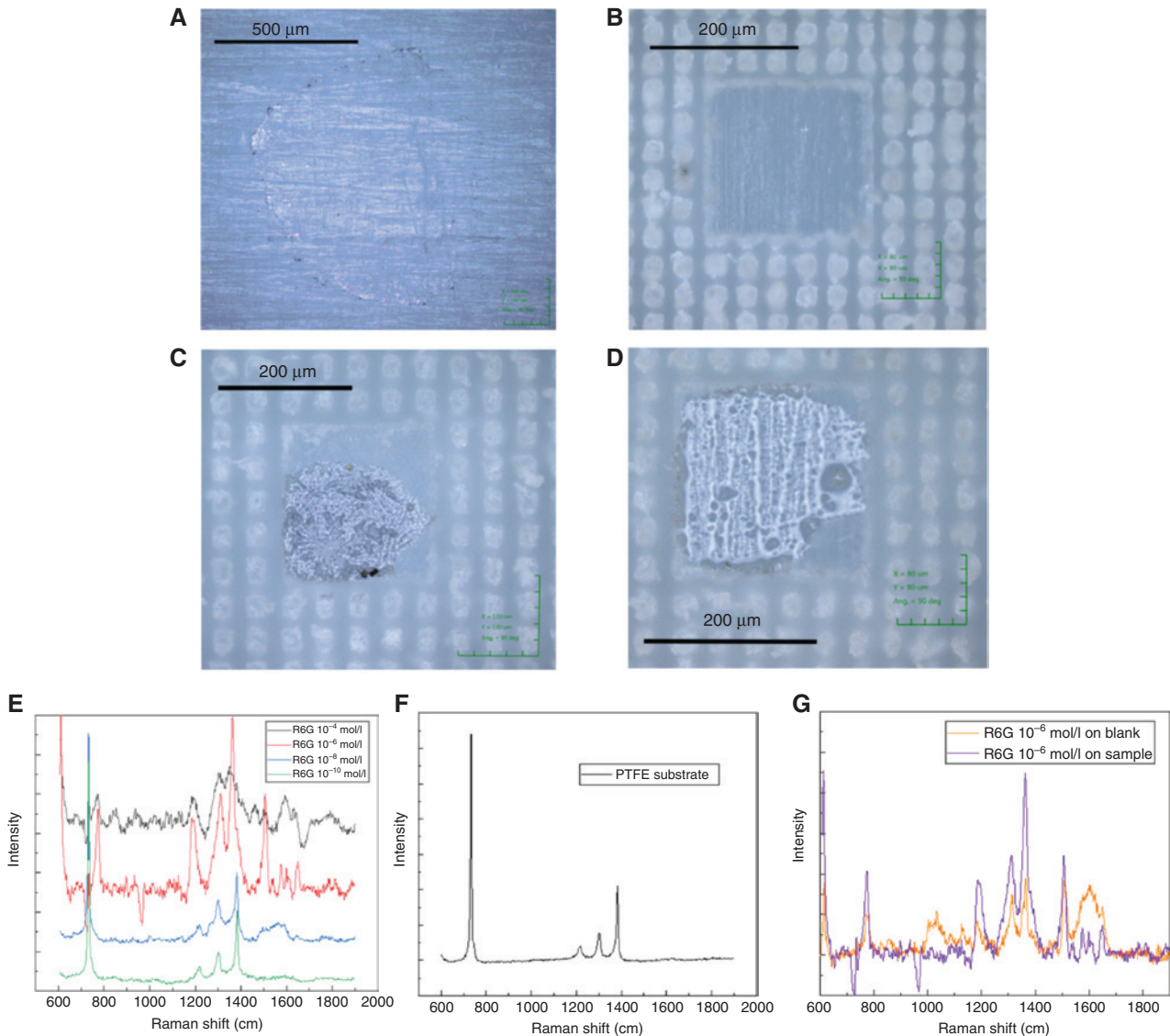


Figure 5: The deposition behaviour on an original PTFE surface (A), clean PTFE droplet trapping zone (B), concentration results on laser-processed sample surfaces with 50 μm scanning interval (C) and 40 μm scanning interval (D), respectively, the Raman spectra of R6G aqueous solution with various concentration mixed with gold sol deposited on laser-processed surfaces (E), of a clean original PTFE surface (F) and of 10^{-6} mol/l R6G aqueous solution mixed with gold sol deposited on a processed PTFE sample and an unprocessed Si wafer, respectively (G).

ring is induced by the differential evaporation rates across the droplet and the resulting outward flow which carries nearly all the solute to the edge [30]. The final contact area is a subround zone with 600–700 μm in diameter, and its area can be approximately calculated to be

$$S = \pi \cdot \left(\frac{650 \mu\text{m}}{2} \right)^2 = 331831 \mu\text{m}^2 \quad (4)$$

In contrast, the laser-processed samples (shown as Figure 5C and D) concentrate all solute into the designed unprocessed square droplet trapping domain without the appearance of coffee ring. The final contact area of these samples can be considered as the area of the

trapping domain, which is only about 14% of that of the unprocessed sample.

$$S' = (235 \mu\text{m})^2 = 55225 \mu\text{m}^2 \quad (5)$$

Zhizhchenko et al. [29] proposed the conception of concentration factor k_c in their research, which is defined as

$$k_c = \frac{V_o}{S_d} \quad (6)$$

where V_o is the initial droplet volume and S_d is the deposition area. In this study, when V_o is fixed at 5 μl and S_d is $(235 \mu\text{m})^2 = 55225 \mu\text{m}^2$, the concentration factor reaches

to 90.5 mm. To magnify the obtained final concentration and to augment the concentration factor, attempts to enlarge V_0 have been done and the initial volume reaches to 10 μl . This indicates that k_c attains 181.0 mm. Repeated experiments were presented, and similar results were obtained.

Then, SERS experiments are performed on the surfaces with the optimised processing parameters. A series of concentrations (10^{-4} M, 10^{-6} M, 10^{-8} M and 10^{-10} M, respectively) of R6G solution are homogeneously mixed with 10^{-6} mol/l Au sol solution. 5 μl droplet of each mixed solution is positioned on the clean laser-processed samples exactly above the droplet trapping domains and an unprocessed Si plate as a blank sample, respectively. After evaporation concentration process, SERS characterisation is performed at these concentrated areas for all the PTFE surfaces. The results are shown in Figure 5E, F, and G, respectively. As can be observed in Figure 5E, characteristic peaks of R6G molecule at 612, 774, 1185, 1311, 1364, 1510, 1537, 1570, 1595, and 1652 (cm^{-1}) [31] can be clearly detected on the laser-processed samples with original 10^{-4} M and 10^{-6} M R6G solution concentrated. With original concentration of 10^{-8} M and 10^{-10} M, only sharp peaks at 733, 1215, 1303, and 1383 (cm^{-1}) can be distinguished. These peaks shall be related to PTFE's characteristic peaks compared with the SERS spectrum of the clean PTFE surface, as shown in Figure 5F. The spectrums of the processed PTFE samples with original concentration of 10^{-8} M and 10^{-10} M have more obvious background peaks especially in the range of 1150–1420 cm^{-1} and 1480–1659 cm^{-1} than that of an unprocessed clean PTFE surface. This suggests that the reception of R6G molecules' signal from the deposited samples is too weak to be detected and recorded. Hence, above results show that R6G molecules can be demonstrably detected at 10^{-4} M and 10^{-6} M, but cannot be detected effectively at 10^{-8} M and 10^{-10} M on the processed PTFE surface. Compared with the unprocessed Si surfaces for the 10^{-6} M mixed R6G solution, the intensity of the detected signal on the processed PTFE trapping zone is one or two orders of magnitude greater under the given conditions, suggesting an enhancement for the detection of trace substances (shown as Figure 5G).

Actually, the effect can be improved to higher levels if the droplet trapping domains can be further processed to be smaller and more hydrophilic, so that the density of 'hot spot' in SERS can be elevated. One probable way is to deposit a noble metal film onto the trap domain to increase its hydrophilicity and to obtain a stronger electromagnetic field, which is expected as one of the vital factors in SERS detection, owing to the coupling between the film

and nanoparticles [32]. In addition, increasing the initial droplet volume can also result in a greater concentration and stronger detection for substances with low concentrations. Further work will be done in these aspects.

4 Conclusions

In conclusion, superhydrophobic PTFE surfaces with designed unprocessed tiny domains are fabricated by femtosecond laser and the processing parameters are optimised to achieve surfaces with excellent superhydrophobicity. Droplet evaporation and concentration behaviour of droplets with targeted solute are systematically studied and compared on the optimised superhydrophobic surfaces and the unprocessed blank surfaces, respectively. It shows that the laser fabricated samples exhibit higher evaporation speed due to their stronger ability to maintain the droplet in a sphere shape and with a larger vapor-liquid contact area. In addition, the dissolved solute can be gathered into the designed unprocessed tiny domains during evaporation on the superhydrophobic surfaces, with the concentration factor attaining 181.0 mm. Dilute R6G solution deposited on the processed samples with the concentration as low as 10^{-6} M, with the assistance of 10^{-6} M Au sol solution, can be evidently detected via SERS. The intensity of the detected R6G signals is effectively enhanced by one or two orders of magnitude compared with that of the unprocessed blank samples, demonstrating the promoting effect of superhydrophobicity on the trace substance characterisation.

5 Supplement information

The methods to measure the relevant data and to calculate the volume of the droplet during evaporation can be found in the pdf file in the Supplementary Materials. Movie S1, S2, and S3 are the videos recording the droplet evaporation behaviour on the surfaces of unprocessed PTFE, sample 3 and sample 7, respectively, corresponding to Figure 4A, B, and C.

Acknowledgement: The authors acknowledge the support by the National Key R & D Program of China (Grant No. 2017YFB1104300), the National Natural Science Foundation of China (funder id: <http://dx.doi.org/10.13039/501100001809>, Grant No. 51575309, 51210009, 51905303) and China Postdoctoral Science Foundation (funder id: <http://dx.doi.org/10.13039/501100002858>, Grant No. 2018M641343).

References

- [1] P. Fan, B. Bai, G. Jin, H. Zhang and M. Zhong, *Appl. Surf. Sci.* 457, 991–999 (2018).
- [2] K. M. Tanvir Ahmmed, J. Montagut and Anne-Marie Kietzig, *Can. J. Chem. Eng.* 95, 1934–1942 (2017).
- [3] W. Liu, P. Fan, M. Yong, X. Luo, C. Chen, et al., *Nanoscale* 11, 8940 (2019).
- [4] Y. Y. Yan, N. Gao and W. Barthlott, *Adv Colloid Interface Sci.* 169, 80–105 (2011).
- [5] P. Papadopoulos, L. Mammen, X. Deng, D. Vollmer and H. Butt, *Proc. Natl. Acad. Sci. U.S.A* 110, 3254–3258 (2013).
- [6] H. Kusumaatmaja, M. L. Blow, A. Dupuis and J. M. Yeomans, *EPL* 81, 36003 (2008).
- [7] R. K. Annavarapu, S. Kim, M. Wang, A. J. Hart and H. Sojoudi, *Sci. Rep.* 9, 405 (2019).
- [8] R. G. Picknett and R. Bexon, *J. Colloid Interface Sci.* 61, 336–350 (1977).
- [9] G. Mchale, S. Aqil, N. J. Shirtcliffe, M. I. Newton and H. Y. Erbil, *Langmuir* 21, 11053–11060 (2005).
- [10] H. Gelderblom, Á. G. Marin, H. Nair, A. van Houselt, L. Letterts, et al., *Phys. Rev. E* 83, 026306 (2011).
- [11] S. A. Kulinich and M. Farzaneh, *Appl. Surf. Sci.* 255, 4056–4060 (2009).
- [12] B. J. Zhang, K. J. Kim and C. Y. Lee, *Exp. Therm. Fluid Sci.* 96, 216–223 (2018).
- [13] Y. Yamada and A. Horibe, *Phys. Rev. E* 97, 043113 (2018).
- [14] S. Dash and S. V. Garimella, *Langmuir* 29, 10785–10795 (2013).
- [15] Y. Gao, N. Yang, T. You, C. Zhang and P. Yin, *Sens. Actuators, B: Chem.* 267, 129–135 (2018).
- [16] F. Guo, H. Yang, J. Mao, J. Huang, X. Wang, et al., *Compos. Commun.* 10, 151–156 (2018).
- [17] Y. Song, T. Xu, L-P. Xu and X. Zhang, *Nanoscale* 10, 20990–20994 (2018).
- [18] Y. Zhang, C. Yang, B. Xue, Z. Peng, Z. Cao, et al., *Sci. Rep.* 8, 898 (2018).
- [19] Y. Wang, M. Wang, L. Shen, Y. Zhu, X. Sun, et al., *Chin. Phys. B* 27, 17801–017801 (2018).
- [20] G. C. Shi, M. L. Wang, Y. Y. Zhu, L. Shen, W. L. Ma, et al., *Sci. Rep.* 8, 6916 (2018).
- [21] S. Y. Chou, C. C. Yu, Y. T. Yen, K. T. Lin, H. L. Chen, et al., *Anal. Chem.* 87, 6017–6024 (2015).
- [22] F. Gentile, G. Das, M. L. Coluccio, F. Mecarini, A. Accardo, et al., *Microelectron. Eng.* 87, 798–801 (2010).
- [23] F. Gentile, M. L. Coluccio, E. Rodanina, S. Santoreillo, D. Di Mascolo, et al., *Microelectron. Eng.* 111, 272–276 (2013).
- [24] A. Millionis, D. Fragouli, L. Martiradonna, G. C. Anyfantis, P. Davide Cozzoli, et al., *ACS Appl. Mater. Interfaces* 6, 1036–1043 (2014).
- [25] W. Song, D. Psaltis and K. B. Crozier, *Lab. Chip* 14, 3907–3911 (2014).
- [26] F. De Angelis, F. Gentile, F. Mecarini, G. Das, M. Moretti, et al., *Nat. Photonics* 5, 682–687 (2011).
- [27] J. E. George, V. K. Unnikrishnan, D. Mathur, S. Chidangil and S. D. George, *Sens. Actuators, B. Chem.* 272, 485–493 (2018).
- [28] F. Chu, S. Yan, J. Zheng, H. Zhang, K. Yu, et al., *NRL* 13, 244 (2018).
- [29] A. Zhizhchenko, A. Kuchmizhak, O. Vitrik, Y. Kulchin and S. Juodkazis, *Nanoscale* 10, 21414–21424 (2018).
- [30] R. D. Deegan, O. Bakajin, T. F. Dupont, G. Huber, S. R. Nagel, et al., *Nature* 389, 827–829 (1997).
- [31] E. C. Le Ru, E. Blackie, M. Meyer and P. G. Etchegoin, *J. Phys. Chem. C* 111, 13794–13803 (2007).
- [32] Y. Fang and Y. Huang, *Appl. Phys. Lett.* 102, 153108 (2013).

Supplementary Material: The online version of this article offers supplementary material (<https://doi.org/10.1515/aot-2019-0072>).